Published in final edited form as:
Int J Quantum Chem. 2012 December 15; 112(24): 3807–3814. doi:10.1002/qua.24237.

Molecular Determinants for Ligand Binding at Serotonin 5-HT$_{2A}$ and 5-HT$_{2C}$ GPCRs: Experimental Affinity Results Analyzed by Molecular Modeling and Ligand Docking Studies

Tania Córdova-Sintjago, **Rajeev Sakhuja**, **Krishnakanth Kondabolu**, **Clinton E. Canal**, and **Raymond G. Booth**
Department of Medicinal Chemistry. College of Pharmacy, University of Florida, Gainesville, Florida 32610

Tania Córdova-Sintjago: taniacsintjago@ufl.edu

Abstract

Ligands that activate the serotonin 5-HT$_{2C}$ G protein-coupled receptor (GPCR) may be therapeutic for psychoses, addiction, and other neuropsychiatric disorders. Ligands that are antagonists at the closely related 5-HT$_{2A}$ GPCR also may treat neuropsychiatric disorders; in contrast, 5-HT$_{2A}$ activation may cause hallucinations. 5-HT$_{2C}$-specific agonist drug design is challenging because 5-HT$_2$ GPCRs share 80% transmembrane (TM) homology, same second messenger signaling, and no crystal structures are reported. To help delineate molecular determinants underlying differential binding and activation of 5-HT$_2$ GPCRs, 5-HT$_{2A}$, and 5-HT$_{2C}$ homology models were built from the β_2-adrenergic GPCR crystal structure and equilibrated in a lipid phosphatidyl choline bilayer performing molecular dynamics simulations. Ligand docking studies at the 5-HT$_2$ receptor models were conducted with the (2*R*, 4*S*)- and (2*S*, 4*R*)-enantiomers of the novel 5-HT$_{2C}$ agonist/5-HT$_{2A/2B}$ antagonist *trans*-4-phenyl-*N,N*-dimethyl-2-aminotetralin (PAT) and its 4′-chlorophenyl congners. Results indicate PAT–5-HT$_2$ molecular interactions especially in TM domain V are important for the (2*R*, 4*S*) enantiomer, whereas, TM domain VI and VII interactions are more important for the (2*S*, 4*R*) enantiomer.

Keywords

serotonin 5-HT$_{2A}$; 5-HT$_{2C}$; GPCR; ligand–receptor interactions; homology modelling; docking; molecular dynamics; phosphatidyl choline bilayer; drug design

Introduction

The neurotransmitter serotonin (5-hydroxytryptamine, 5-HT) mediates some of its diverse physiological and psychological effects by activation of the 5-HT$_2$ family of G protein-coupled receptors (GPCRs) that consists of the 5-HT$_{2A}$, 5-HT$_{2B}$, and 5-HT$_{2C}$ subtypes. Drugs that activate 5-HT$_{2C}$ receptors are in development for psychoses, addiction, and other neuropsychiatric disorders, as well as, obesity.[1,2] Meanwhile, most currently used antipsychotic drugs are antagonists at the 5-HT$_{2A}$ receptor.[2] In contrast, activation of 5-HT$_{2A}$ receptors is associated with hallucinogenic effects.[3] Moreover, activation of 5-HT$_{2B}$ receptors causes cardiopulmonary toxicity.[4] Thus, there is essentially no clinical tolerance for activation of 5-HT$_{2A}$ and 5-HT$_{2B}$ receptors. Development of 5-HT$_{2C}$-specific agonist

Correspondence to: Tania Córdova-Sintjago, taniacsintjago@ufl.edu.

drugs, however, is challenging because 5-HT_2 receptors share about 80% transmembrane (TM) sequence identity[5] and same second messenger signaling. Moreover, there are no three-dimensional (3D) crystal structures for any of the 5-HT_2 GPCs.

G-protein coupled receptors have a similar 3D structure consisting of a bundle of seven TM alpha helices, connected by alternating intracellular and extracellular loops, with the N-terminus in the extracellular domain and C-terminus in the intracellular domain. About 900 GPCRs are known, however, crystal structures are known only for the following: bovine rhodopsin (bRho),[6–10] opsin,[11,12] human A_{2A} adenosine receptor,[13] turkey β_1 adrenoceptor,[14] human β_2 adrenoceptor (β_2AR) in an inactive state,[15–17] β_2AR in a nanobody-stabilized active-state,[18] β_2AR in complex with an irreversible agonist,[19,20] human dopamine D_3 receptor in complex with a agonist,[21] and human H_1 receptor in a complex with an antagonist at 3.1 Å (PDB code 3RZE).[22] The recent X-ray structure of an antagonist bound to the A_{2A} receptor confirms ligands bind deep in the orthosteric site binding pocket.[23]

In the absence of crystal structures for most GPCRs, mutagenesis studies are used to characterize ligand–receptor molecular interactions and to validate GPCR receptor models and ligand docking studies. Thus, it is known that ligand binding at serotonin 5-HT_2 and other monoaminergic GPCRs requires ionic interaction between a ligand positively charged amine moiety and the carboxylate of the fully conserved aspartate residue D3.32.[24–28] For example, we recently reported that mutation of D3.32 to alanine (D3.32A) in the 5-HT_{2C} GPCR abolishes detectable binding of the radioligand [^{3}H]-mesulergine.[29] This and other experimental results helped to validate ligand docking and molecular dynamics (MDs) results using a 5-HT_{2C} receptor model built by homology to the human β_2AR.[29,30]

In this work, we sought to compare overall receptor structures and ligand binding sites that could underlie ligand differential binding and activation of 5-HT_2 GPCRs for drug development purposes. Accordingly, we built a 5-HT_{2A} receptor homology model based on the structure the human β_2AR (PDB code 2*R*h1), using methods analogous to those used to obtain a 5-HT_{2C} homology model.[30] Docking studies were carried on the model receptors for the (2*R*, 4*S*)- and (2*S*, 4*R*)-enantiomers of the novel 5-HT_{2C} agonist/5-$HT_{2A/2B}$ antagonist *trans*-4-phenyl-*N*,*N*-dimethyl-2-aminotetralin (PAT)[24] and its 4′-chlorophenyl congners (4′-Cl-PAT). PAT–5-HT_2 molecular interactions that lead to receptor subtype differential binding and activation are discussed relative to drug design.

Methods

Model building

A homology model of the human serotonin 5-HT_{2A} receptor was built based on the crystal structure of the β_2AR/T4-lysozyme chimera (Protein Data bank entry 2RH1),[17] in similar method used to obtain the 5-HT_{2C} homology model.[30] In brief, the 5-HT_{2A} native sequence was aligned to the β_2AR sequence using *ClustalW* multiple sequence alignment.[31,32] The inverse agonist, carazolol present in the β_2AR crystal structure was removed, as well as T4, cholesterol and other molecules present in the β_2AR/T4-lysozyme chimera. Point mutations were performed as needed and the gaps were analyzed, followed by the appropriate sequence additions and deletions to match the 5-HT_{2A} receptor aminoacid sequence. The TM domains were built using the Biopolymer module of *Sybyl-X 1.3*.[33] The crude model of the unbound receptor was minimized using the Powell method implemented in *Sybyl* with Tripos force field [34] and AMBER charges.[35] The resulting model was equilibrated in a 1-palmitoyl-2-oleyl-*sn*-glycero phosphatidyl choline (POPC) bilayer.[36] The system was relaxed using the Tripos force field to a gradient 0.05 Kcal/Å mol, prior to MDs simulation in the POPC membrane. MD simulation conditions were time run 5 μs,

time step 1 fs, with snapshots collected every 5 fs. Other parameters were the NVT (constant number of particles N, Volume V, and Temperature T) canonical ensemble, 300 K temperature, Boltzmann initial velocities, and nonbonded cutoff set at 8 Å. Constraints for alpha carbons in the TM domains were employed. Subsequently, the constraints were removed for a 1000 ps MD simulation run. The final unbound 5-HT_{2A} homology model was obtained from the median structure after clustering analysis of the frames from the last 10 ps. of the MDs simulation, and optimized using the Tripos force field to a convergence of 0.05 Kcal/Å mol.

Ligands and docking

Synthesis, absolute configuration (based on X-ray crystal structure), and pharmacology of (2*R*, 4*S*)- and (2*S*, 4*R*)-PAT and 4′-Cl-PAT (Fig. 1) are reported elsewhere.[37,38] The ligand structures were built as monocations (protonated amines) using *HyperChem 8.0* [39] and structures were optimized using PM3 model Hamiltonian to a gradient of 0.01 Kcal/Å mol.

Ligands were pre-positioned in the binding pocket by performing rigid docking with the *PatchDock* server.[40] The low-energy-high-score solutions were analyzed to select the initial configuration, ensuring the essential interaction between the carboxylate oxygen of receptor residue D3.32 and the ligand protonated amine moiety.[20,22] The initial ligand-receptor complex configuration was used for flexible ligand docking with *Flexidock* in *Sybyl-x 1.2*.[33] *Flexidock* uses an algorithm to probe the conformational space defining possible interactions between the ligand and its putative binding site. The binding site was defined by assigning residue D3.32 as a definitive binding site interaction point, and including residues within a 7 Å radius. Structure preparation was performed prior to docking studies assigning AMBER[35] charges for the protein and Gesteiger– Marsili [41] charges for the ligand. Rotatable bonds in the ligand and the side chains of residues defining the receptor putative active site were screened for optimal positioning of the ligand and side chains in the conformational space; remaining residues were frozen during docking. Default *FlexiDock* parameters were set at 80,000-generation. The best docking solution, according to the highest *FlexiDock* score, was minimized using the Tripos force field to a gradient 0.05 Kcal/Å mol, prior to MDs simulation. The selected high-score pose of the docked ligand was subjected to a MD simulation run for 500 ps, with other parameters the same as above, to allow adjustment of the positions of side-chains and helices. The final structure of the ligand docked into the receptor was obtained from the average of last 10 ps of the dynamics simulation.

Results and Discussion

Homology modeling and 5-HT_{2A}, 5-HT_{2C} receptor comparison

The first step in the homology model building involves the sequence of the WT 5-HT_{2A} receptor was aligned to the sequence of the template structure β_2A receptor using *ClustalW*. Sequence alignment showing the TM domains is shown in Table 1, the 5-HT_{2C} receptor sequence is also shown in the alignment. Conserved residues are indicated in bold, and reference residues are labeled according to the standard Ballesteros nomenclature for GPCRs.[42]

The TM alignment shows the very close similarity between the 5-HT_{2A} and -HT_{2C} GPCRs.

The β_2AR has been used to build homology models of several related GPCRs including the 5-HT_{2C} receptor; the latter homology model was validated by site-directed mutagenesis and ligand binding studies.[29,30] Despite the low overall sequence identity between the β_2A and

both 5-HT_{2A} and 5-HT_{2C} receptors (~30%), the majority of highly conserved residues among these GPCRs are in the TM helices, thus allowing for accurate alignment.

Conserved residue sequences among 5-HT_2 receptors and the β_2AR receptor in the TM domains were used to verify the alignment, comprising: **GN**X**LVI** motif in TM I, including the reference residue N1.50, **TNYF**, **SLA**X**AD** motifs in TM II, including the reference residue **D2.50**, **DVL** motif in TM III, including the essential residue **D3.32**, **TASI**, and **DRY** motifs, also in TM III, **KA** motif and reference residue **W4.50** in TM IV, **F**XX**PL**X**IM** motif in TM V, including **P5.50**, **W**X**PFFI**X**NI** motif in TM VI, including residues **W6.48**, and reference residue **P6.50**, and **WIGY** and **NPL**X**Y** motifs in TM VII, including reference residue **P7.50**.

The alignment in Table 1 was used to generate the 3D model of the WT 5-HT_{2A}, as described above, suing the method used to build the 5-HT_{2C} homology models based on β2AR crystal structure 2Rh1. The resulting TM bundle structure of the WT 5-HT_{2A} receptor is shown in Figure 2, generated with *PyMOL 1.3*.[43] TMH are spectrum-color-coded, from blue for TM I, to red for TM VII. In Figure 2, panel A shows the TM bundle oriented with the extracellular domain on top and the intracellular domain at the bottom. Panel B is the view from the extracellular domain down into the receptor cavity.

The resulting 5-HT_{2A} model was analyzed using *PDBsum* in *PROCHECK 3.6*.2.[44,45] Figure 3 shows the Ramachandran plot for the 5-HT_{2A} model; *PROCHECK* statistics are reported in Table 2. Analysis of the Ramachandran plot results show 97.3% of residues are in the allowed regions, 84.1% are in the most favored regions (Psi angle values vary −180 to 0°; Phi angle values vary 0 to 180°; bottom-left quadrant, Fig. 3), and 12.4% are in additional allowed regions; supplementary 0.8% are in generously allowed regions, confirming the quality of the model.

5-$HT2_A$–5-HT_{2C} receptor structure analysis

Superposition of the 5-HT_{2A} and -5HT_{2C} GPCR structures was performed by selecting all alpha carbons as superposition criteria, in *Sybyl-x 1.2*.[33] The root-mean-square deviation (RMSD) 1.879 Å overall suggests close similarity between these structures (Fig. 4, Panel A).

Additional comparison of the structures was performed by aligning the alpha carbons of binding pocket residues conserved in each of the structures, that is, D3.32, S3.36, W6.48, F6.51, F6.52, N6.55, and Y7.43. The RMSD result was 0.4932 Å, indicating the binding pocket of these structures are very analogous (Fig. 4, Panel B).

Ligand affinity and docking at 5-HT_{2A} AND 5-HT_{2C} receptors

Affinity of (2S, 4R) and (2R, 4S)-PAT and 4′-Cl-PAT at 5-HT_{2A} and 5-HT_{2C} GPCRs—The experimentally determined affinity values (Ki) for (2*R*, 4*S*)- and (2*S*, 4*R*)-PAT and 4′-Cl-PAT at human WT 5-HT_{2A} and 5-HT_{2C} receptors[24,38] are summarized in Table 3.

Stereochemistry apparently plays an important role in binding of PAT and 4′-Cl-PAT at 5-HT_{2A} and 5-HT_{2C} receptors. Moreover, electronic as well as steric parameters of the 4-phenyl-2-aminotetralin scaffold impact stereoselective 5-HT_2 binding and function. For example, at both 5-HT_{2A} and 5-HT_{2C} receptors, higher affinity is associated with the (2*S*, 4*R*)-configuration of PAT whereas it is the (2*R*, 4*S*)-enantiomer of 4′-Cl-PAT that has higher affinity (Table 3). Regarding function, agonist activity at 5-HT_{2C} receptors is observed for both PAT and 4′-Cl-PAT, regardless of stereochemistry. At 5-HT_{2A} receptors, however, function appears to be sensitive to stereochemistry and perhaps other electronic

and steric parameters associated with the 4-phenyl-2-aminotetralin scaffold; thus, agonist activity is observed only for (2*R*, 4*S*)-PAT (Table 3).

Docking of (2S, 4R-) and (2R, 4S)-PAT at 5-HT$_{2A}$ and 5-HT$_{2C}$ GPCRs—To help interpret the experimental data in Table 3, ligand docking studies were undertaken to delineate ligand– receptor molecular interactions for (2*S*, 4*R*)- and (2*R*, 4*S*)-PAT at the 5-HT$_{2A}$ and 5-HT$_{2C}$ receptor models. Figure 5 shows the more active (2*S*, 4*R*)-enantiomer of PAT docked at each model.

At the 5-HT$_{2A}$ model (Fig. 5A), the protonated amine group of (2*S*, 4*R*)-PAT could form a bifurcated hydrogen bond (HB) with the carboxylate oxygen atoms of 5-HT$_{2A}$ residue D3.32 (bonding distance 2.02–2.30 Å), which also could form an HB with the *para*-hydroxy group of Y7.43 (bonding distance 1.40 Å). The C(4) phenyl group of (2*S*, 4*R*)-PAT docked close to the F6.52 phenyl sidechain (bonding distance 4.2 Å), however, the orientation does not favor π-π interactions.

At the 5-HT$_{2C}$ model (Fig. 5B), the protonated amine group of (2*S*, 4*R*)-PAT could form a bifurcated HB with the carboxylate of D3.32 (bonding distance 1.77–2.22 Å), over a shorter distance than was observed at the 5-HT$_{2A}$ model. The 5-HT$_{2C}$ D3.32 moiety also could form an HB with the *para*-hydroxy group of Y7.43 (bonding distance 1.56 Å), as is the case for 5-HT$_{2A}$, and, also could form an HB with the hydroxy group of S3.36 (bonding distance 1.58 Å). Moreover, at the 5-HT$_{2C}$ receptor model (in contrast to the 5-HT$_{2A}$ model), the aromatic part of the PAT tetrahydronaphthalene system docked close and parallel to the aromatic ring of Y7.32 (bonding distance 3.7 Å; Fig. 5B), which could facilitate π–π interactions. Meanwhile, the (2*S*, 4*R*)-PAT C(4) phenyl moiety docked in a hydrophobic pocket formed by 5-HT$_{2C}$ residues W6.48, F6.51, and F6.52 (Fig. 5B), as observed in previously studies.[29,30] Thus, in comparison to the 5-HT$_{2A}$ receptor, there are additional aromatic and hydrophobic interactions possible between (2*S*, 4*R*)-PAT and the 5-HT$_{2C}$ receptor that likely account for its three-times higher affinity at 5-HT$_{2C}$ compared to 5-HT$_{2A}$ receptors (Table 3).

In comparison to (2*S*, 4*R*)-PAT, the (2*R*, 4*S*)-PAT enantiomer binds with lower affinity at both 5-HT$_{2A}$ and 5-HT$_{2C}$ receptors (Table 3) and docking results are helpful to explain the observed experimental data. For example, when (2*R*, 4*S*)-PAT was docked at the 5-HT$_{2A}$ receptor model (not shown), its protonated amine moiety could form an HB with D3.32 at a slightly longer distance (1.80–3.37 Å) than was observed for (2*S*, 4*R*)-PAT, however, the (2*R*, 4*S*)-PAT C(4) phenyl ring and tetrahydronaphthyl system docked relatively far (7.0 Å) from 5-HT$_{2A}$ binding pocket aromatic residues W6.48, F6.51, and F6.52, presumably, precluding significant binding interactions with these residues. When (2*R*, 4*S*)-PAT was docked at the 5HT$_{2C}$ model (not shown), its protonated amine moiety was relatively far (2.45 Å) from the receptor D3.32 residue, and its C(4) phenyl moiety was far (6.6–7.0 Å) from the 5-HT$_{2C}$ binding pocket aromatic residues W6.48, F6.51, and F6.52, precluding hydrophobic or π–π interactions. Overall, in comparison to the (2*S*, 4*R*)-PAT enantiomer, docking results reveal a significant lack of potential binding interactions between the (2*R*, 4*S*)-PAT enantiomer and the 5-HT$_{2A}$ and 5-HT$_{2C}$ receptor models, that likely explains the lower affinity of this enantiomer at both receptors (Table 3).

Docking of (2S, 4R) and (2R, 4S)-4′-Cl-PAT at 5-HT$_{2A}$ and 5-HT$_{2C}$ GPCRs—For comparison to the PAT binding and docking results reported above, (2*S*, 4*R*)-Cl-PAT (Fig. 6) and (2*R*, 4*S*)-4′-Cl-PAT (Fig. 7) were each docked at the 5-HT$_{2A}$ and 5-HT$_{2C}$ receptor models; for clarity, only the binding pocket amino acid residues of the receptor are shown. When (2*S*, 4*R*)-4′-Cl-PAT was docked at the 5-HT$_{2A}$ model (Fig. 6A), it was apparent that a bifurcated HB could form with the D3.32 carboxylate (bonding distance 1.83–1.96 Å),

which, could also form an HB with the indol sidechain of W3.28 (bonding distance 1.78 Å), but, not with Y7.38. When (2*S*, 4*R*)-4′-Cl-PAT was docked at the 5-HT_{2C} model (Fig. 6B), a single HB could form with D3.32 (bonding distance 1.77 Å), which, also could form an HB with the indol side-chain of W3.28 (bonding distance 1.78 Å) and with the hydroxy sidechain of Y7.43 (bonding distance 1.36 Å). There were no apparent interactions observed between the 4′-Cl-substituent of (2*S*, 4*R*)-4′-Cl-PAT and the 5-HT_{2A} or 5-HT_{2C} receptor models.

When (2*R*, 4*S*)-4′-Cl-PAT was docked at the 5-HT_{2A} model (Fig. 7A), it was apparent that the protonated amine could form an HB with the carboxylate sidechain of D3.32 (bonding distance 1.75 Å) over a shorter distance than was found for the (2*S*, 4*R*)-4′-Cl-PAT enantiomer. Also, D3.32 could form an HB with the hydroxy group of Y7.43 (bonding distance 1.49 Å). The 4′-Cl-substituent of (2*R*, 4*S*)-4′-Cl-PAT could interact with the hydroxy sidechain of S5.43 (bonding distance 2.50 Å).

When (2*R*, 4*S*)-4′-Cl-PAT was docked to the 5-HT_{2C} model (Fig. 7B), its protonated amine moiety could form an HB to D3.32 (bonding distance 1.60 Å), which could also form an HB with Y7.43 (bonding distance 1.48 Å). As observed for the 5-HT_{2A} receptor, the 4′-Cl-substituent of (2*R*, 4*S*)-4′-Cl-PAT also oriented close to the hydroxyl moiety of 5-HT_{2C} residue S5.43 (bonding distance 2.50 Å). Thus, at both 5-HT_{2A} and 5-HT_{2C} receptors, the interaction of the 4′-Cl-substituent of (2*R*, 4*S*)-4′-Cl-PAT with the S5.43 residue, together, with the potential for a close and presumably tight HB with D3.32, likely explains the higher affinity of this enantiomer over the (2*S*, 4*R*)-4′-Cl-PAT enantiomer at 5-HT_{2A} and 5-HT_{2C} receptors (Table 3).

Conclusions

Computational studies were performed to build βAR-based homology models of the 5-HT_{2A} and 5-HT_{2C} GPCRs for ligand docking studies, to characterize 3D (stereochemical) molecular determinants for binding of drug candidates. Ligand–receptor interactions in the binding pocket were analyzed and compared to the experimentally determined affinity values (Ki) at both 5-HT_{2A} and 5-HT_{2C} GPCRs. The higher affinity of (2*S*, 4*R*)-PAT at 5-HT_{2C} *versus* 5-HT_{2A} receptors was rationalized in light of modeling results indicating the ligand could form significant π–π interactions with the 5-HT_{2C} Y7.43 residue, but, not with the corresponding 5-HT_{2A} Y7.43 residue. The observed reversed stereoselective affinity of PAT and 4′-Cl-PAT at 5-HT_{2A} and 5-HT_{2C} receptors (Table 3) was rationalized in view of docking results indicating that (2*R*, 4*S*)-4′-Cl-PAT could form a close and presumably tight HB with the D3.32 residue of both receptors. Meanwhile, the corresponding (2*R*, 4*S*)-PAT enantiomer docked relatively far away from the 5-HT_2 residue D3.32 compared to the other ligands, and, the same is true for its C(4) phenyl ring and tetrahydronaphthyl system regarding interactions with 5-HT_2 binding pocket aromatic residues W6.48, F6.51, and F6.52.

It has been suggested that 5-HT_2 residue Y7.43 plays a role in stabilizing the negative charge of the D3.32 carboxylate, and, this interaction is more or less, depending on the ligand structure and conformation/activation state of the receptor.[29,30] In this work, we found that binding of PAT analogs to the 5-HT_{2A} or 5-HT_{2C} receptor decreased the distance between the receptor Y7.43 hydroxy moiety and D3.32 carboxylate moiety; the exception was (2*S*, 4*R*)-4′-Cl-PAT, where no closer interaction between these residues was observed upon binding of the ligand. It is not yet clear how D3.32–Y7.43 interaction upon ligand binding may impact ligand affinity or resulting functional activity.

Homology modeling incorporating MD simulations leads to improved results when all-atom MD simulations and relatively long simulation times with sufficiently accurate force fields are used.[46] Thus, in the present work we used all-atom MD simulations of the receptor embedded in a pre-equilibrated POPC system to emulate the membrane, with simulation times of 5 μs. We have obtained improved accuracy regarding the predictions of such models, for example, the β2-AR based-homology model of the human histamine H_1 receptor, built using a protocol analogous to the one resented in this work, was compared with the human H_1 crystal structure, with resulting RMSD 2.91 Å.[47] This result suggests the present methodology produces reliably predictable homology models, useful for the study of drug–receptor interaction for drug design purposes.

Acknowledgments

Contract grant sponsor: National Institutes of Health; Contract/grant numbers: RO1 DA023928, DA030989, and MH081193.

References

1. Jensen NH, Cremers TI, Sotty F. Sci World J. 2010; 10:1870.
2. Bubar MJ, Cunningham KA. Prog Brain Res. 2008; 172:319. [PubMed: 18772040]
3. Nichols DE. Pharmacol Ther. 2004; 101:131. [PubMed: 14761703]
4. (a) Fitzgerald LW, Burn TC, Brown BS, Patterson JP, Corjay MH, Valentine PA, Sun JH, Link JR, Abbaszade I, Hollis JM, Largent BL, Hartig PR, Hollis GF, Meunier PC, Robichaud AJ, Robertson DW. Mol Pharmacol. 2000; 57:75. [PubMed: 10617681] (b) Launay JM, Herve P, Peoc'h K, Tournois C, Callebert J, Nebigil CG, Etienne N, Drouet L, Humbert M, Simonneau G, Maroteaux L. Nat Med. 2000; 8:1129. [PubMed: 12244304] (c) Rothman RB, Baumann MH, Savage JE, Rauser L, McBride A, Hufeisen SJ, Roth BL. Circulation. 2000; 102:2836. [PubMed: 11104741]
5. Kroeze WK, Kristiansen K, Roth BL. Curr Top Med Chem. 2002; 2:507. [PubMed: 12052191]
6. Palczewski K, Kumasaka T, Hori T, Behnke CA, Motoshima H, Fox BA, Trong IL, Teller DC, Okada T, Stenkamp RE, Yamamoto M, Miyano M. Science. 2000; 289:793.
7. Li J, Edwards PC, Burghammer M, Villa C. J Mol Biol. 2004; 343:1409. [PubMed: 15491621]
8. Okada T, Sugihara M, Bondar AN, Elstner M, Entel P, Buss V. J Mol Biol. 2004; 342:571. [PubMed: 15327956]
9. Okada T, Fujiyoshi Y, Silow M, Navarro J, Landau EM, Shichida Y. Proc Natl Acad Sci USA. 2002; 99:5982. [PubMed: 11972040]
10. Teller DC, Okada T, Behnke CA, Palczewski K, Stenkamp RE. Biochemistry. 2001; 40:7761. [PubMed: 11425302]
11. Park JH, Scheerer P, Hofmann KP, Choe HW, Ernst OP. Nature. 2008; 454:183. [PubMed: 18563085]
12. Scheerer P, Park JH, Hildebrand PW, Kim YJ, Krauss N, Choe HW, Hofmann KP, Ernst OP. Nature. 2008; 455:497. [PubMed: 18818650]
13. Jaakola VP, Griffith MT, Hanson MA, Cherezov V, Chien EYT, Lane JR, Ijzerman AP, Stevens RC. Science. 2008; 322:1211. [PubMed: 18832607]
14. Warne T, Serrano-Vega MJ, Baker JG, Moukhametzianov R, Edwards PC, Henderson R, Leslie AGW, Tate CG, Schertler GFX. Nature. 2008; 454:486. [PubMed: 18594507]
15. (a) Cherezov V, Rosenbaum DM, Hanson MA, Rasmussen SGF, Thian FS, Kobilka TS, Choi HJ, Kuhn P, Weis WI, Kobilka BK, Stevens RC. Science. 2007; 318:1258. [PubMed: 17962520] (b) Rosenbaum DM, Cherezov V, Hanson MA, Rasmussen SGF, Thian FS, Kobilka TS, Choi HJ, Yao XJ, Weis WI, Stevens RC, Kobilka BK. Science. 2007; 318:1266. [PubMed: 17962519]
16. Hanson MA, Cherezov V, Griffith MT, Roth CB, Jaakola VP, Chien EY, Velasquez J, Kuhn P, Stevens RC. Structure. 2008; 16:897. [PubMed: 18547522]

17. Rasmussen SG, Choi HJ, Rosenbaum DM, Kobilka TS, Thian FS, Edwards PC, Burghammer M, Ratnala VR, Sanishvili R, Fischetti RF, Schertler GF, Weis WI, Kobilka BK. Nature. 2007; 450:383. [PubMed: 17952055]
18. Rassmussen SG, Choi HJ, Fung JJ, Pardon E, Casarosa P, Chae PS, DeVree BT, Rosembaum DM, Thian FS, Kobilka TS, Schnapp A, Konetzki I, Sunahara RK, Gellman SH, Pautsch A, Steyaert J, Weis WI, Kobilka BK. Nature. 2011; 469:175. [PubMed: 21228869]
19. Rosembaum DM, Zhang C, Lyons JA, Holl R, Aragao D, Arlow DH, Rasmussen SG, Choi HJ, DeVree BT, Sunahara RK, Chae PS, Gellman SH, Dror RO, Shaw DE, Weis WI, Caffrey M, Gmeiner P, Kobilka BK. Nature. 2011; 469:236. [PubMed: 21228876]
20. Congreve M, Langmea CJ, Mason JS, Marshall FH. J Med Chem. 2011; 54:4283. [PubMed: 21615150]
21. Chien EYT, Liu W, Zhao Q, Katritch V, Han GW, hanson MA, Shi L, Newman AH, Javitch JA, Cherezov V, Stevens RC. Science. 2010; 330:1091. [PubMed: 21097933]
22. Schimamura T, Shiroishi M, Weyand S, Tsujimoto H, Winter G, Katritch V, Abagyan R, Cherezov V, Liu W, Won Han G, Kobayashi T, Stevens RC, Iwata S. Nature. 2011; 475:65. [PubMed: 21697825]
23. Congreve M, Andrews SP, Dore AS, Hollenstein K, Hurrell E, Langmead CJ, Mason JS, Ng IW, Tehan B, Zhukov A, Weir M, Marshall FH. J Med Chem. 2012; 55:1898. [PubMed: 22220592]
24. Booth RG, Fang L, Huang Y, Wilczynski A, Sivendran S. Eur J Pharmacol. 2009; 615:1. [PubMed: 19397907]
25. Bucholtz EC, Brown RL, Tropsha A, Booth RG, Wyrick SD. J Med Chem. 1999; 42:3041. [PubMed: 10447948]
26. Kristiansen K, Dahl SG. Eur J Pharmacol. 1996; 306:195. [PubMed: 8813633]
27. Kristiansen K, Kroeze WK, Willins DL, Gelber EI, Savage JE, Glennon RA, Roth BL. J Pharmacol Exp Ther. 2000; 293:735. [PubMed: 10869371]
28. Booth RG, Fang L, Wilczynski A, Sivendren S, Sun Z, Travers S, Bruysters M, Sansuk K, Leurs R. Inflam Res. 2008; 57(suppl 1):S43.
29. Canal C, Cordova-Sintjago TC, Villa NY, Fang LJ, Booth RG. Eur J Pharmacol. 2011; 673:1. [PubMed: 22020288]
30. Cordova-Sintjago T, Villa N, Canal C, Booth R. Int J Quantum Chem. 2011; 112:140.
31. Thompson JD, Higgins DG, Gibson TJ. Nucleic Acids Res. 1994; 22:4673. [PubMed: 7984417]
32. Larkin MA, Blackshields G, Brown NP, Chenna R, McGettigan PA, McWilliam H, Valentin F, Wallace IM, Wilm A, Lopez R, Thompson JD, Gibson TJ, Higgins DG. Bioinformatics. 2007; 23:2947. [PubMed: 17846036]
33. SYBYL-X 1.2. Tripos International; 1699 South Hanley Rd., St. Louis, Missouri, 63144, USA:
34. Clark M, Cramer RD III, van Opdenhosch N. J Comput Chem. 1989; 10:982.
35. Cornell WD, Cieplak P, Bayly CI, Gould IR, Merz KM Jr, Ferguson DM, Spellmeyer DC, Fox T, Caldwell JW, Kollman PA. J Am Chem Soc. 1995; 117:5179.
36. Heller H, Schaefer M, Schulten K. J Phys Chem. 1993; 97:8343.
37. Wyrick SD, Booth RG, Myers AM, Owens CE, Kula NS, Baldessarini RJ, McPhail AT, Mailman RB. J Med Chem. 1993; 36:2542. [PubMed: 8102651]
38. Sakhuja R, Kondobolu K, Canal CE, Cordova-Sintjago T, Kim MS, Sun Z, Vincek AS, Travers S, Abboud KA, Booth RG. J Med Chem. (submitted for publication).
39. HyperChem (TM) Professional 8.0. Hypercube, Inc; 1115 NW 4th Street, Gainesville, Florida 32601, USA:
40. Schneidman-Duhovny D, Inbar Y, Nussinov R, Wolfson HJ. Nucleic Acids Res. 2006; 33:W363. [PubMed: 15980490]
41. Gasteiger J, Marsili M. Tetrahedron. 1980; 36:3219.
42. (a) Ballesteros JA, Jensen AD, Liapakis G, Rasmussen SG, Shi L, Gether U, Javitch JA. J Biol Chem. 2001; 276:29171. [PubMed: 11375997] (b) Ballesteros JA, Shi L, Javitch JA. Mol Pharmacol. 2001; 60:1. [PubMed: 11408595]
43. The PyMOL Molecular Graphics System, Version 1.3. Schrödinger, LLC;

44. Laskowski RA, MacArthur MW, Moss DS, Thornton JM. J Appl Crystallogr. 1993; 26:283.
45. Morris AL, MacArthur MW, Hutchinson EG, Thornton JM. Proteins. 1992; 12:345. [PubMed: 1579569]
46. Raval A, Piana S, Eastwood MP, Dror RO, Shaw DE. Proteins Struct Funct Bioinform. 201210.1002/prot.24098
47. Cordova-Sintjago, T.; Fang, L.; Bruysters, M.; Leurs, R.; Booth, R. 243rd ACS national meeting; San Diego, California. 2012. MEDI 214

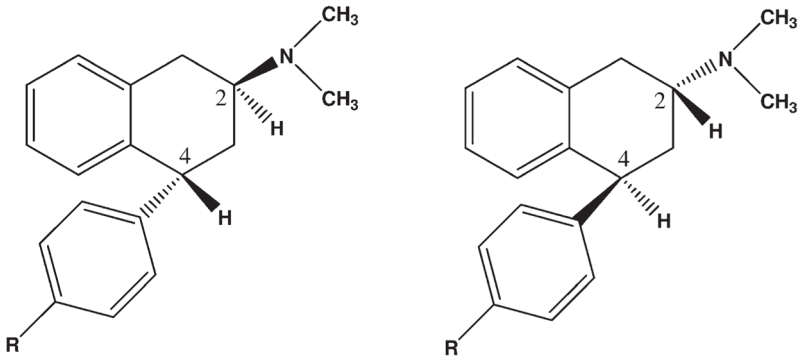

R = H (2*S*, 4*R*)-PAT
R = Cl (2*S*, 4*R*)-PAT

R = H (2*R*, 4*S*)-PAT
R = Cl (2*R*, 4*S*)-PAT

Figure 1.
PATs used in 5-HT_{2A} and 5-HT_{2C} docking studies.

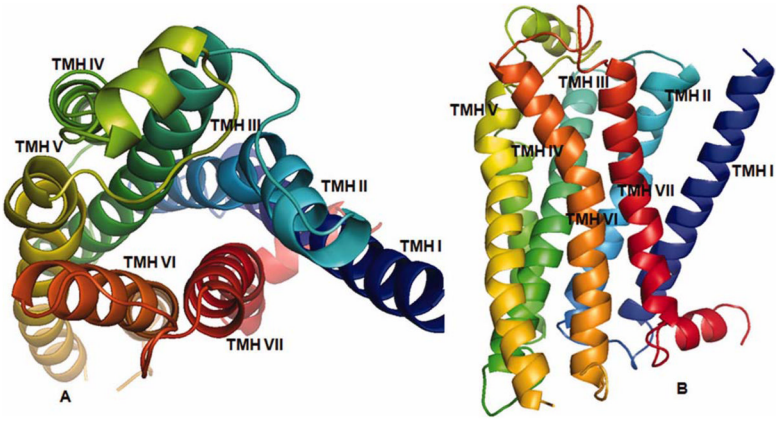

Figure 2.

3D 5-HT_{2A} model structure: Panel A: TM domains with the extracellular domain on top, and the intracellular domain at the bottom. Panel B: View from the extracellular domain showing the binding site cavity. [Color figure can be viewed in the online issue, which is available at wileyonlinelibrary.com.]

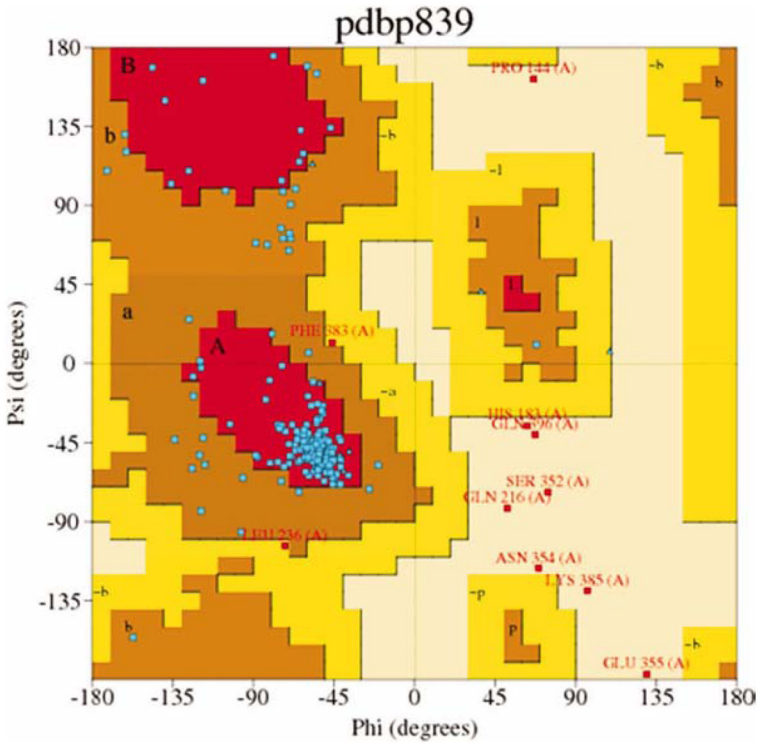

Figure 3.

Ramachandran Plot of the β2AD-based 5-HT_{2A} homology model generated with PROCHECK. [Color figure can be viewed in the online issue, which is available at wileyonlinelibrary.com.]

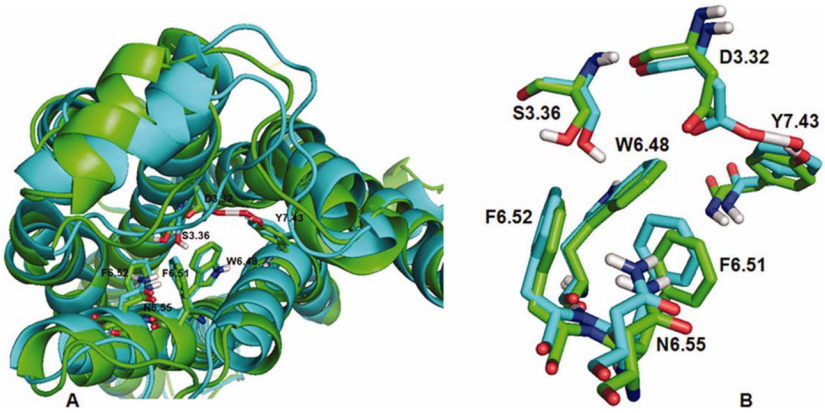

Figure 4.

Comparison of 5-HT_{2A} (green ribbons) and 5-HT_{2C} (blue ribbons) GPCR models. Panel A: GPCRs are oriented with extracellular domains at top and intracellular domains at bottom, overall RMSD = 1.88 Å. Panel B: Superimposition conserved residues in the binding pocket is shown, RMSD = 0.49 Å. [Color figure can be viewed in the online issue, which is available at wileyonlinelibrary.com.]

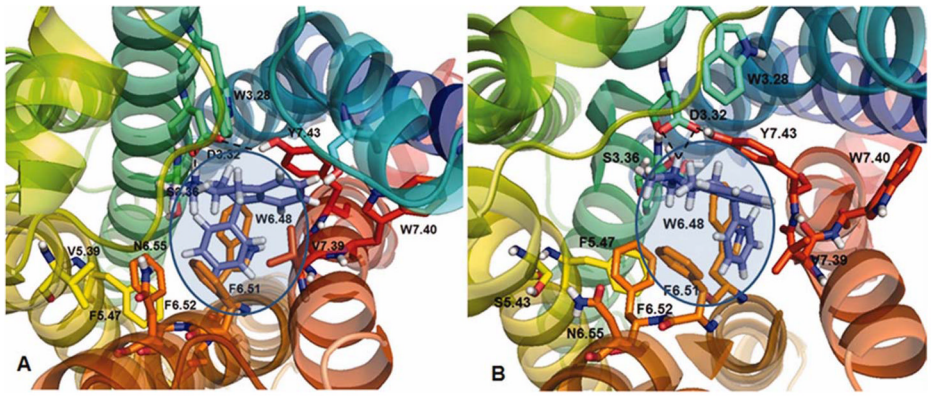

Figure 5.

(2*S*, 4*R*)-PAT docked at 5-HT_{2A} (panel A) and 5-HT_{2C} (panel B) receptor models. The binding pocked is showed as shaded area. Dashed lines indicate ionic and HB interactions. [Color figure can be viewed in the online issue, which is available at wileyonlinelibrary.com.]

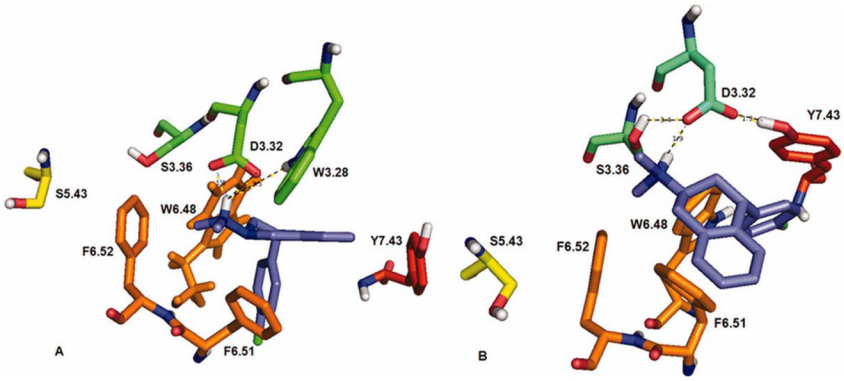

Figure 6.
(2*S*, 4*R*)-4′-Cl-PAT docked at 5-HT_{2A} (panel A) and 5-HT_{2C} (panel B) receptor models. Only the binding pocket amino acid residues of the receptor are shown for clarity. [Color figure can be viewed in the online issue, which is available at wileyonlinelibrary.com.]

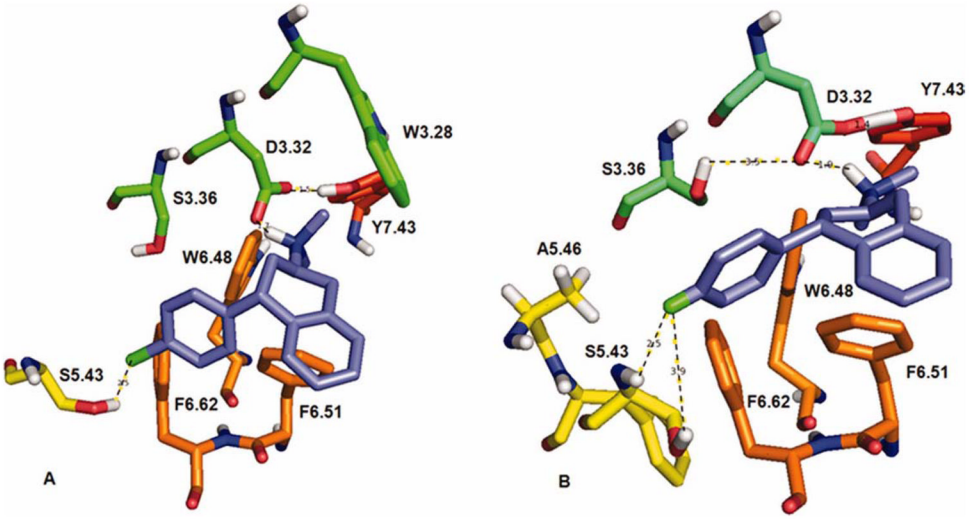

Figure 7.
(2*R*, 4*S*)-4′-Cl-PAT docked at 5-HT_{2A} (panel A) and 5-HT_{2C} (panel B) receptor models. Only the binding pocket amino acid residues of the receptor are shown for clarity. [Color figure can be viewed in the online issue, which is available at wileyonlinelibrary.com.]

Table 1

Alignment of 5-HT_{2C} 5-HT_{2C} and β2AR GPCRs sequences using *ClustalW*.

```
                                                                N1.50
5HT2A_HUMAN      NRTNLSCEGCLSPSCLSLLHLQEKNWSALLTAVVIILTIAGNILVIMAVS 100
5HT2C_HUMAN      GRFKFPDG--------------VQNWPALSIVIIIIMTIGGNILVIMAVS 79
ADRB2_HUMAN      ----------------------------IVMSLIVLAIVFGNVLVITAIA 59
                                  D2.50
5HT2A_HUMAN      LEKKLQNATNYFLMSLAIADMLLGFLVMPVSMLTILYGYRWPLPSKLCAV 150
5HT2C_HUMAN      MEKKLHNATNYFLMSLAIADMLVGLLVMPLSLLAILYDYVWPLPRYLCPV 129
ADRB2_HUMAN      KFERLQTVTNYFITSLACADLVMGLAVVPFGAAHILMK-MWTFGNFWCEF 108

                     D3.32             R3.50             K4.41    W4.50
5HT2A_HUMAN      WIYLDVLFSTASIMHLCAISLDRYVAIQNPIHHSRFNSRTKAFLKIIAVW 200
5HT2C_HUMAN      WISLDVLFSTASIMHLCAISLDRYVAIRNPIEHSRFNSRTKAIMKIAIVW 179
ADRB2_HUMAN      WTSIDVLCVTASIETLCVIAVDRYFAITSPFKYQSLLTKNKARVIILMVW 158
                                                                S5.43
                     P5.50   Y5.58
5HT2A_HUMAN      SFFIPLTIMVITYFLTIKSLQKEATLCVSDLGTRAKLASFSFLP------ 285
5HT2C_HUMAN      AFFIPLTIMVITYCLTIYVLRRQALMLLHGHTEEPPGLSLDFLKCCKRNT 271
ADRB2_HUMAN      SFYVPLVIMVFVYSRVFQEAKRQLQKIDKS-------------------- 236

                 K6.35        W6.48  N6.55                    Y7.43
5HT2A_HUMAN      KVLGIVFFLFVVMWCPFFITNIMAVICKESCNEDVIGALLNVFVWIGYLS 372
5HT2C_HUMAN      KVLGIVFFVFLIMWCPFFITNILSVLCEKSCNQKLMEKLLNVFVWIGYVC 360
ADRB2_HUMAN      KTLGIIMGTFTLCWLPFFIVNIVHVIQDNLIRKEVYILLN----WIGYVN 318
                     P7.50
5HT2A_HUMAN      SAVNPLVYTLFNKTYRSAFSRYIQCQYKENKKP-LQLILVNTIPALAYKS 421
5HT2C_HUMAN      SGINPLVYTLFNKIYRRAFSNYLRCNYKVEKKPPVRQIPRVAATALSGRE 410
ADRB2_HUMAN      SGFNPLIYCRS-PDFRIAFQELLCLRRSSLKAYGNGYSSNGNTGEQSGYH 367
```

Conserved residues are indicated in bold. Reference residues are labeled according to Ballesteros nomenclature [42].

Table 2

Recheck statistics of TM residues in the 5-HT_{2A} homology model.

	Number of residues	%
Most favored regions	217	84.1
Additional allowed regions	32	12.4
Generously allowed regions	2	0.8

Table 3

Affinity of PAT and 4′-Cl-PAT at 5-HT_{2A} and 5-HT_{2C} GPCRs.

	K_i ± SEM (nM)	
Ligand	**5-HT_{2A}**	**5-HT_{2C}**
(2*R*, 4*S*)-PAT	460 ± 47	500 ± 70
(2*S*, 4*R*)-PAT	95 ± 7.2	27 ± 2.6
(2*R*, 4*S*)-4′-Cl-PAT	42 ± 6.0	45 ± 7.0
(2*S*, 4*R*)-4′-Cl-PAT	240 ± 32	130 ± 16